

Geophysical Research Letters

RESEARCH LETTER

10.1029/2019GL082458

Key Points:

- Squeezing and stretching of density layers modulates the diapycnal diffusion of oceanic tracers
- Squeeze dispersion enhances dispersion by 2–3 times across some isopycnals in the abyssal Samoan Passage
- Diapycnal transport is strongly affected by positive correlations between squeezing and turbulence

Supporting Information:

- Supporting Information S1

Correspondence to:

G. L. Wagner,
gregory.leclaire.wagner@gmail.com

Citation:

Wagner, G. L., Flierl, G., Ferrari, R., Voet, G., Carter, G. S., Alford, M. H., & Girton, J. B. (2019). Squeeze dispersion and the effective diapycnal diffusivity of oceanic tracers. *Geophysical Research Letters*, 46, 5378–5386. <https://doi.org/10.1029/2019GL082458>

Received 2 MAR 2019

Accepted 22 APR 2019

Accepted article online 29 APR 2019

Published online 21 MAY 2019

Squeeze Dispersion and the Effective Diapycnal Diffusivity of Oceanic Tracers

Gregory L Wagner¹ , Glenn Flierl¹, Raffaele Ferrari¹, Gunnar Voet² , Glenn S Carter³, Matthew H Alford² , and James B Girton⁴ 

¹Earth, Atmospheric, and Planetary Sciences, Massachusetts Institute of Technology, Cambridge, MA, USA, ²Scripps Institution of Oceanography, University of California, San Diego, La Jolla, CA, USA, ³Department of Oceanography, University of Hawai'i at Manoa, Honolulu, HI, USA, ⁴Applied Physics Laboratory, University of Washington, Seattle, WA, USA

Abstract We describe a process called “squeeze dispersion” in which the squeezing of oceanic tracer gradients by waves, eddies, and bathymetric flow modulates diapycnal diffusion by centimeter to meter-scale turbulence. Due to squeeze dispersion, the effective diapycnal diffusivity of oceanic tracers is different and typically greater than the average “local” diffusivity, especially when local diffusivity correlates with squeezing. We develop a theory to quantify the effects of squeeze dispersion on diapycnal oceanic transport, finding formulas that connect density-averaged tracer flux, locally measured diffusivity, large-scale oceanic strain, the thickness-weighted average buoyancy gradient, and the effective diffusivity of oceanic tracers. We use this effective diffusivity to interpret observations of abyssal flow through the Samoan Passage reported by Alford et al. (2013, <https://doi.org/10.1002/grl.50684>) and find that squeezing modulates diapycnal tracer dispersion by factors between 0.5 and 3.

Plain Language Summary Turbulent vertical ocean mixing forms a key part of the Earth’s climate system by drawing atmospheric carbon and heat into the massive reservoir that is the deep ocean. Quantifying vertical ocean mixing is difficult: vertical mixing is associated with turbulence at the tiny scales of centimeters to meters but affects the entire ocean on the long time scales of decades and centuries. We demonstrate that vertical ocean mixing depends not *only* on small-scale turbulence, but on the *combination* of small-scale turbulence and larger-scale motions, such as currents, eddies, and waves similar to the jet streams and hurricanes of the atmosphere. In particular, when a patch of ocean is mixed by small-scale turbulence while being “squeezed” in the vertical at the same time by currents and eddies, the patch ultimately mixes more quickly than the turbulence would cause alone. This means that estimating the total rate of oceanic vertical mixing requires knowledge both of the magnitude of ocean squeezing as well as the intensity of small-scale ocean turbulence.

1. Introduction

Squeeze dispersion is a process in which the diapycnal diffusion of tracers such as dissolved carbon, temperature, salinity, oxygen, nutrients, and plankton is modulated in fluctuating flows that alternately squeeze material surfaces together and stretch them apart. Squeeze dispersion, called “accelerated diffusion” by Moffatt (1983), is a nonturbulent process relevant to flows that have moderate strain but lack the crinkling, rolling up, and exponential stretching of material surfaces associated with turbulent mixing. Squeeze dispersion plays a role in flows under strong geometric or dynamical constraints: for example, low Reynolds flows confined by solid boundaries, or stratified, rotating, and anisotropic planetary flows.

In this paper we investigate the effects of strain and squeeze dispersion on turbulent diffusion across density surfaces in the Earth’s ocean, where strong density stratification typically limits turbulent diapycnal mixing to “microscales” smaller than ten meters. The small scales of diapycnal mixing mean that the effect of diapycnal mixing on “macroscale” vertical tracer transport over hundreds to thousands of meters can be characterized by an inhomogeneous “local” turbulent diffusivity. In this context, squeeze dispersion occurs when fluctuating macroscale tracer gradients due to fluctuating strain lead to a discrepancy between the average local diffusivity and the “bulk” effective tracer diffusivity. Macroscale flows associated with strain and squeeze dispersion include mesoscale and submesoscale eddies, fronts, and large-scale internal waves.

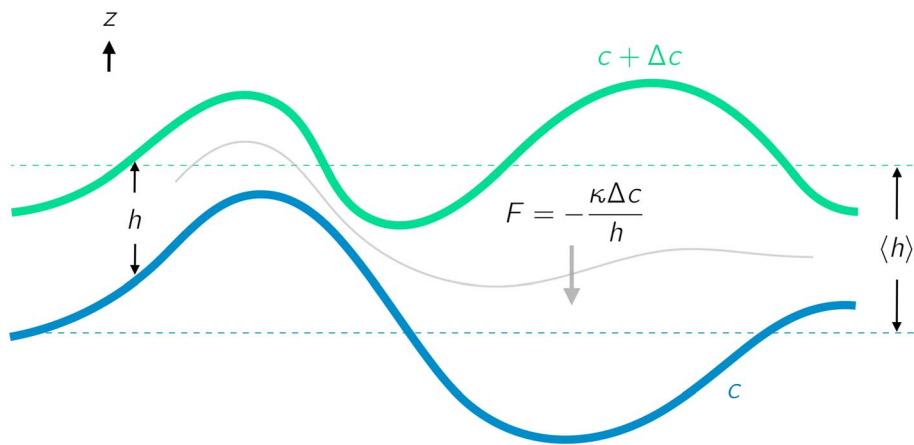


Figure 1. Squeeze dispersion between two isotracer surfaces with tracer concentrations c and $c + \Delta c$. The diffusive flux between the fluctuating surfaces is $F = -\kappa \Delta c/h$, where h is the separation between the surfaces and κ is the local diffusivity across the layer. The spatially averaged separation between the two surfaces is $\langle h \rangle$. Introducing an effective squeeze dispersion diffusivity $\kappa_e = \langle h \rangle (\kappa/h)$ implies that $\langle F \rangle = -\kappa_e \Delta c / \langle h \rangle$.

An estimate for the vertical diffusive flux across a squeezed macroscale layer of fluid illustrates the basic mechanism of squeeze dispersion. In this scenario, depicted in Figure 1, a layer of fluid between material and isotracer surfaces with concentrations c and $c + \Delta c$ is squeezed and stretched by a macroscale flow with strain but no overturning. Microscale turbulent mixing across the layer associated with overturning on scales much smaller than the separation between the two surfaces is characterized by the vertical diffusive flux $F = -\kappa \Delta c/h$, where κ is the isotropic turbulent diffusivity and h is the vertical separation between the surfaces.

The average vertical tracer flux across the layer is $\langle F \rangle = -\Delta c \langle \kappa/h \rangle$, where the angle brackets denote a layer-following average that encompasses fluctuations in both h and κ . This formula for $\langle F \rangle$ reflects the intuitive fact that, relative to a fixed κ distribution, an increase in squeezing and thus variations in h acts to increase the average flux $\langle F \rangle$ across the layer. Increasing diffusive flux with increasing strain is the hallmark of squeeze dispersion. To express $\langle F \rangle$ in terms of the average separation between the surfaces $\langle h \rangle$, we introduce the effective diffusivity,

$$\kappa_e = \langle h \rangle \left\langle \frac{\kappa}{h} \right\rangle, \quad (1)$$

such that $\langle F \rangle = -\kappa_e \Delta c / \langle h \rangle$.

The squeeze dispersion effective diffusivity in (1) is derived using a particular average that follows the vertical motion of a strained layer of fluid. Squeeze dispersion and the effects of strain on tracer diffusion, however, do not depend on the averaging method used to quantify their effect. We make this point concrete in section 2, where we show that the effective diffusivity in (1) describes the dispersion of a tracer patch advected by barotropic flow over undulating bathymetry. We show further in section 3 that (1) arises in the thickness-weighted-average equation (10) for the dispersion of tracers on the scales of ocean circulation.

The effective diffusivity in (1) is a bulk diapycnal diffusivity obtained by averaging tracer flux over macroscale fluctuations and along isopycnals and dividing the result by the thickness-weighted-average tracer gradient. This interpretation of (1) in terms of tracer fluxes suggests a method for analyzing microstructure observations that makes use of Osborn's (1980) hypothesized relationship between turbulent dissipation rate and buoyancy flux: rather than "averaging κ ," the computation of (1) requires averaging the buoyancy flux $\Gamma \epsilon$ along surfaces or layers of constant density, where Γ is the mixing coefficient, the proportionality constant between turbulent dissipation rate ϵ and local buoyancy flux.

In section 4, we implement this method for calculating κ_e in (1) in an analysis of microstructure observations from the Samoan Passage and find that the effective diapycnal diffusivity of tracers advected through the Samoan passage differs from the local diffusivity averaged on isopycnals by factors of 0.5–3. This difference between bulk effective diffusivity and average local diffusivity in the Samoan passage suggests that realistic variations in diffusivity and squeezing can modulate the dispersion of oceanic tracers and may contribute to

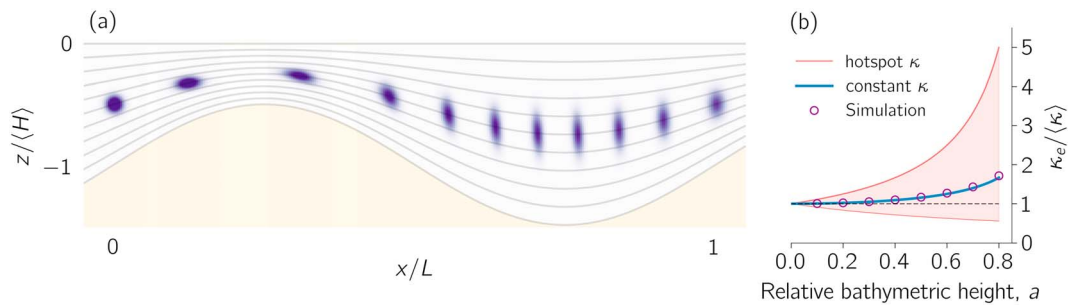


Figure 2. (a) Time-lapse of tracer patch advection in a numerical solution to (2)–(4) with $a = 0.5$. (b) Modulation of diffusion by squeeze dispersion in a numerical solution to (2)–(4) (purple circles) with constant κ , the theoretical prediction 7 with constant κ (blue line), and the theoretical prediction for mixing “hot spots” located at the point of maximum squeezing ($\kappa \propto \delta(x + L/4)$; upper red line) and the point of maximum stretching ($\kappa \propto \delta(x + 3L/4)$; lower red line). Red shading indicates the range of possible modulation of diffusion by squeezing in this problem, and a gray dashed line indicates $\kappa_e/\langle \kappa \rangle = 1$. We use $U = 1$, $\langle H \rangle = 1$, $L = 20$, $\kappa = 10^{-4} \text{ m}^2/\text{s}$ and tracer initial condition $c(t = 0) = \exp[-x^2/2\ell^2 - (z + \langle H \rangle/2)^2/2d^2]/2\pi\ell d$ with $\ell = L/100$ and $d = \langle H \rangle/20$.

differences between tracer-based and microstructure-based estimates of diapycnal diffusivity inferred from observations as, for example, in the Brazil Basin (Ledwell et al., 2000), the East Pacific sector of the Antarctic Circumpolar Current (Ledwell et al., 2011), and Drake Passage (Mashayek et al., 2017; St. Laurent et al., 2012; Watson et al., 2013).

2. Squeeze Dispersion in Flow Over Undulating Bathymetry

The squeeze dispersion process is illustrated by the advection of a diffusing tracer patch through the contracting streamlines of a two-dimensional flow $u(x), w(x, z)$. The effects of microscale turbulent mixing on tracer dispersion are modeled by an inhomogeneous turbulent diffusivity, $\kappa(x, z, t)$. The tracer concentration $c(x, z, t)$ then obeys the advection-diffusion equation

$$c_t + uc_x + wc_z = \partial_x(\kappa c_x) + \partial_z(\kappa c_z), \quad (2)$$

where the barotropic horizontal and vertical velocity are

$$u(x) = \frac{U}{H} \quad \text{and} \quad w(x, z) = \frac{zUH_x}{H^2}, \quad (3)$$

with barotropic transport U , length L , depth

$$H(x) = \langle H \rangle \left[1 - a \sin\left(\frac{2\pi x}{L}\right) \right], \quad (4)$$

average depth $\langle H \rangle$, and nondimensional relative bathymetric height a . Figure 2a shows a time lapse of an initially Gaussian tracer patch with $\int c dx dz = 1$ squeezed and stretched by the flow in (3) with constant κ .

We compare $\langle \kappa \rangle$ to the measured effective diffusivity

$$\kappa_e \stackrel{\text{def}}{=} (2T)^{-1} \int (Z - z)^2 c dx dz, \quad (5)$$

where $Z = \int z c dx dz$ is the z centroid of the tracer patch, based on the change in the vertical variance of the tracer patch after one cycle of periodic squeezing. The identical configuration of the streamlines in the periodic bathymetric flow at $t = 0$ and $x = 0$, and $T = \langle H \rangle L/U$ and $x = L$ allows us to compute the change in tracer vertical variance in z coordinates and avoid the complications of streamline coordinates that would be required in a more complicated flow. The definition of κ_e was introduced by Aris (1956) and is used to interpret oceanic tracer release experiments such as that reported by Ledwell et al. (2011). In Figure 2b, the ratio between the numerically measured effective diffusivity κ_e and the prescribed constant diffusivity κ is plotted with purple circles, showing how $\kappa_e/\langle \kappa \rangle \geq 1$ and how squeeze dispersion always increases κ_e over a constant κ . This is squeeze dispersion: tracer dispersion increases with increasing a and thus increasing squeezing, despite acceleration of the tracer patch over the constriction and stretching over the contraction.

The nature of squeeze dispersion is revealed by a special solution to (2)–(3) derived in the supporting information in which we assume the tracer patch has a thin aspect ratio such that $\partial_x(\kappa c_x) \ll \partial_z(\kappa c_z)$, use a transformation into bathymetric coordinates with the initial condition $c(t = 0) = \delta(x)\delta(z + \langle H \rangle/2)$, and allow turbulent diffusivities of the form $\kappa(x, t)$. The tracer distribution is Gaussian after being advected for a time $t_n = n\langle H \rangle L/U$ through n “squeezing cycles” over the periodic bathymetry,

$$c(t = t_n) = \frac{1}{\sqrt{4\pi\kappa_e t_n}} \exp\left[-\frac{(z + \langle H \rangle/2)^2}{4\kappa_e t_n}\right] \delta(x - nL), \quad (6)$$

and therefore spreads diffusively in the vertical while advected horizontally. The effective diffusivity that determines tracer patch dispersion is

$$\kappa_e = \langle H \rangle \left\langle \frac{\kappa}{H} \right\rangle, \quad \text{where} \quad \langle \phi \rangle \stackrel{\text{def}}{=} \frac{1}{L} \int_0^L \phi dx. \quad (7)$$

The Gaussian shape of c in (6) means that κ_e in (6)–(7) is identical to the effective diffusivity defined in terms of the growth of tracer variance, $\kappa_e = (2T)^{-1} \int (Z - z)^2 c dx dz$. Because $\langle 1/H \rangle \geq 1/\langle H \rangle$ for any positive function $H(x)$, (7) implies that fluctuating squeezing always enhances the diffusive transport associated with a constant κ . Moreover, the enhancement is increased further relative to $\langle \kappa \rangle$ when κ and squeezing positively correlate.

In Figure 2b we compare the diffusivity modulation $\kappa_e/\langle \kappa \rangle$ in numerical solutions to (2) (purple circles) with the theoretical prediction (7) (blue line) versus a . The numerical and analytical solutions show that $\kappa_e/\langle \kappa \rangle > 1$ for constant κ , corresponding to a modest enhancement in tracer diffusion due to squeeze dispersion. The slight disagreement between the numerical and analytical solutions for constant κ is due to the contribution of horizontal diffusion and shear to the vertical dispersion of the patch in the numerical solution. The red solid lines plot (7) for diffusivity “hot spots” associated with $\kappa \propto \delta(x - L/4)$ (upper red line) and $\kappa \propto \delta(x - 3L/4)$ (lower red line) that form upper and lower bounds for the modulation of κ_e due to squeeze dispersion, showing how correlations between squeezing and a nonconstant κ can act to either reduce or significantly enhance the tracer effective diffusivity κ_e relative to $\langle \kappa \rangle$.

3. Squeeze Dispersion and the Circulation of Oceanic Tracers

Next we show that squeeze dispersion affects the diapycnal diffusion of tracers on the scales of ocean circulation in depth-dependent stratification and flow. For this we use a series of two averages introduced by both De Szoeke and Bennett (1993) and Young (2012) to obtain a description of the circulation of oceanic tracers that distinguishes between advection by the residual-mean circulation, isopycnal dispersion by mesoscale eddies, and diapycnal squeeze dispersion by microstructure turbulence.

We first apply a spatial “microscale average” over turbulent fluctuations on scales of centimeters to $O(10)$ m. The microscale average (*i*) yields a monotonic density field and enables the use of buoyancy coordinates and (*ii*) permits the turbulent closure $\tilde{\mathbf{u}}\tilde{c} = -\kappa \nabla c$ for the average microscale turbulent flux $\tilde{\mathbf{u}}\tilde{c}$, where $\tilde{\mathbf{u}}$ is the microscale velocity field, \tilde{c} is the microscale tracer concentration, κ is the microscale turbulent diffusivity, and (c) is the “macroscale” tracer gradient. The macroscale tracer concentration c then obeys

$$c_t + \mathbf{u} \cdot \nabla c = \nabla \cdot (\kappa \nabla c), \quad (8)$$

where the advecting velocity field \mathbf{u} includes large-scale internal waves as well as submesoscale, quasi-geostrophic, and bathymetric flows with vertical scales larger than 10 m.

We introduce a second, thickness-weighted “macroscale average” defined for any variable ϕ via

$$\hat{\phi} \stackrel{\text{def}}{=} \frac{\langle h\phi \rangle}{\langle h \rangle}. \quad (9)$$

In (9), $h \stackrel{\text{def}}{=} g/b_z$ is the “thickness” of the buoyancy surface $b = -g\rho'/\rho_0$, where g is gravitational acceleration, ρ_0 is a reference potential density, and ρ' is the potential density perturbation therefrom. The angle brackets in (9) denote an ensemble, time, or spatial average over macroscale fluctuations in buoyancy coordinates (Young, 2012). Our results are strictly true only for ensemble averages, but time or spatial averages may be used to similar but approximate effect where ensembles of oceanic motion are not available

(Davis, 1994). Averaging in buoyancy coordinates is crucial for distinguishing between fundamental circulation processes: advection of tracer by the residual velocity, stirring of tracers along mean isopycnal surfaces by mesoscale eddies, and mixing across mean density surfaces by microscale turbulence.

We show in the supporting information that applying the thickness-weighted average in (9) to the macroscale tracer equation (8) leads to an equation for the evolution of tracers on the scales of ocean circulation:

$$\left(\partial_t + \mathbf{u}^* \cdot \nabla - \underbrace{\partial_z \langle h \rangle \left\langle \frac{\kappa}{h} \right\rangle \partial_z}_{\stackrel{\text{def}}{=} \kappa_e} \right) \hat{c} = -\nabla \cdot \mathbf{E}^c. \quad (10)$$

Equation (10) describes the dispersion of the large-scale tracer concentration \hat{c} due to advection by the circulation velocity \mathbf{u}^* , stirring and diffusion by macroscale eddy fluxes \mathbf{E}^c defined in supporting information equation (SI18), and across-isopycnal diffusion due to the effective diapycnal diffusivity $\kappa_e = \langle h \rangle (\kappa/h)$.

Ocean models that employ the Gent and McWilliams (1990) scheme to parameterize mean advection by mesoscale eddies and the Redi diffusivity (Redi, 1982) to parameterize eddy mixing along isopycnals may implicitly use (10) to model the dispersion of oceanic tracers (McDougall & McIntosh, 2001). In these models, the Redi diffusivity acts to parameterize the eddy fluxes \mathbf{E}^c in (10), while the advecting velocity field \mathbf{u}^* is modeled as the sum of a resolved velocity field and a “quasi-Stokes” velocity field (McDougall & McIntosh, 2001) approximated by the Gent and McWilliams (1990) scheme. In these models and in actuality, isopycnal advection and mixing dominate the isopycnal dispersion of oceanic tracers at large scales. Equation (10) demonstrates how diapycnal squeeze dispersion complements isopycnal mixing by eddy fluxes \mathbf{E}^c and residual advection by \mathbf{u}^* to determine the total—along-isopycnal and cross-isopycnal—dispersion of oceanic tracers.

The effective diapycnal diffusivity experienced by oceanic tracers is given by the squeeze dispersion formula $\kappa_e = \langle h \rangle (\kappa/h)$, analogous to the effective diffusivities (1) and (7) emerging in the introduction and the barotropic problem in section 2. The mediation of oceanic tracer diffusion by squeeze dispersion implies an outsized importance for correlations either dynamical or coincidental between squeezing and microscale turbulence.

4. Squeeze Dispersion in the Samoan Passage

To assess the importance of oceanic squeeze dispersion, we compare the effective squeeze diffusivity in (1) and (10) with the average local diffusivity of a hypothetical tracer advected along isopycnals in observations of abyssal flow through the Samoan Passage—a 40-km-wide conduit between the southern and northern Pacific Ocean where strong abyssal flow over rough and constricted bathymetry produces hydraulic jumps, lee waves, turbulence, and squeezing. We focus on the eastern channel of the Samoan Passage using a series of hydrographic and direct turbulence observations made in 2012 and summarized in Figure 3a and by Alford et al. (2013).

Our analysis uses 13 vertical profiles of small-scale shear, temperature, and pressure made by a Rockland Vertical Microstructure Profiler (VMP) whose locations are overlain over contours of Samoan passage bathymetry in Figure 3a. Conductivity was not measured by the VMP, so we estimate VMP salinity with a fifth-order polynomial fit to the temperature-salinity relationship measured by nearby Sea-Bird 911plus conductivity-temperature-depth profiles. The temperature, conductivity, and pressure profiles are adapted to a 1-m grid and used to compute profiles of potential density referenced to pressure at a depth of 4,000 m, which we denote σ . The turbulent kinetic energy dissipation rate, $\epsilon \stackrel{\text{def}}{=} \nu |\nabla \tilde{\mathbf{u}}|^2$, where ν is the kinematic ocean viscosity and $\tilde{\mathbf{u}}$ is the microscale velocity field, is estimated from the VMP data by fitting local shear fluctuation spectra to the Nasmyth spectrum (Oakey & Elliott, 1982) and further integrating following Gregg (1998).

We next define 22 layers equally distributed in density space between $\sigma = 45.85 \text{ kg/m}^3$ and $\sigma = 45.96 \text{ kg/m}^3$ with width $\Delta\sigma = 0.005 \text{ kg/m}^3$. The depth of these 22 density layers ranges from 3,144 to 5,106 m within the 13 VMP profiles. The gridded $\sigma(z)$ profiles and 22 density layers $\sigma_i \pm \frac{1}{2}\Delta\sigma$ are visualized in Figure 3b.

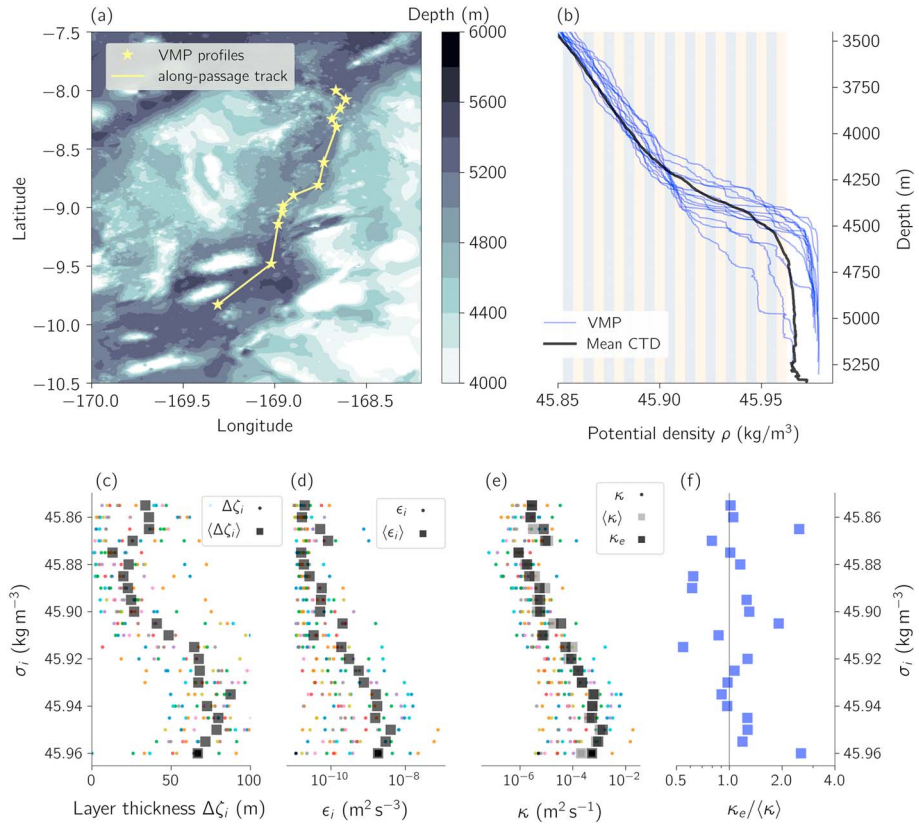


Figure 3. Effect of squeezing on diapycnal dispersion in the Samoan passage. (a) shows Samoan Passage bathymetry and VMP profile locations. (b) VMP density profiles in blue, the mean of 8 passage CTD density profiles in black, and the 22 density layers used for analysis with vertical stripes. (c–e) The profiles and passage averages of layer thickness $\Delta\zeta_i$, layer-averaged turbulent dissipation rate ϵ_i , and cross-layer diffusivity κ_i . Panel (e) also plots effective diffusivity κ_e and (f) plots the ratio $\kappa_e/\langle\kappa\rangle$. VMP = Vertical Microstructure Profiler; CTD = conductivity-temperature-depth.

The vertical extent of each density layer, $\Delta\zeta_i$, and layer-averaged turbulent dissipation, ϵ_i , are computed for each profile by sorting the σ profile to obtain a monotonic, stably stratified density profile $\sigma'(z)$ and permuting ϵ to find ϵ' such that $\epsilon'(\sigma') = \epsilon(\sigma)$. We next invert $\sigma'(z)$ to find $\zeta' = z(\sigma')$, where z is a vertical coordinate that increases upwards to $z = 0$ at the ocean surface, and linearly interpolate ζ' in σ' to determine $\Delta\zeta_i$ via

$$\Delta\zeta_i = \zeta' \left(\sigma_i - \frac{1}{2} \Delta\sigma \right) - \zeta' \left(\sigma_i + \frac{1}{2} \Delta\sigma \right). \quad (11)$$

We compute the layer-averaged dissipation, ϵ_i , from the sorted data by evaluating

$$\epsilon_i(\sigma_i) = \frac{1}{\Delta\sigma} \int_{\sigma_i - \Delta\sigma/2}^{\sigma_i + \Delta\sigma/2} \epsilon'(\sigma') d\sigma', \quad (12)$$

numerically with the trapezoidal rule and using linear interpolation in σ' to estimate ϵ' at the end points $\sigma_i \pm \frac{1}{2} \Delta\sigma$. Finally, we note that the maximum overturn density adjustment $\max(|\sigma' - \sigma|)$ over all profiles is 0.0014 kg/m^3 , smaller than the layer size $\Delta\sigma = 0.005$.

We compute the local diffusivity across each density layer using Osborn's (1980) formula for the relationship between turbulent dissipation and buoyancy flux,

$$\kappa(\sigma_i) \stackrel{\text{def}}{=} \frac{\Gamma \epsilon_i}{N_i^2}, \quad (13)$$

where $\Gamma = 0.2$ is the mixing coefficient, the ratio between microscale buoyancy flux and kinetic energy dissipation. In (13), N_i^2 is the buoyancy gradient across each σ_i layer defined in terms of $\Delta\zeta_i$ via

$$N_i^2 = -\frac{g\Delta\sigma}{\rho_0\Delta\zeta_i}, \quad (14)$$

where $g = 9.81 \text{ m/s}^2$ is gravitational acceleration and $\rho_0 = 1,045.85 \text{ kg/m}^3$.

We develop a bulk average by defining an along-passage track that connects the 13 VMP stations with straight lines in latitude-longitude coordinates, and defining an along-passage coordinate “ x ” that increases along the track from south to north. The along-passage track connecting VMP stations is shown in Figure 3a. We define an average of any variable $\phi(x, \sigma_i)$ within a density layer σ_i and along the Samoan passage as

$$\langle \phi \rangle(\sigma_i) \stackrel{\text{def}}{=} \frac{1}{L} \int_0^L \phi(x, \sigma_i) dx, \quad (15)$$

where x is distance on the along-passage track in Figure 3a and L is the total length of path connecting the VMP profiles. The integral in (15) is estimated from the discrete data using the trapezoidal rule. In Figures 3c–3e, we compare the profiles and passage averages of $\Delta\zeta_i$, ϵ_i , and κ , respectively.

We use (15) to compute the effective diffusivity in (1) and (10), $\kappa_e = \langle h \rangle \langle \kappa/h \rangle$, where the thickness is defined $h = g/N^2$ in terms of the local buoyancy gradient N^2 and gravitational acceleration g . This definition of the effective diffusivity with the average in (15) is reminiscent of the definition that appears in the effective diffusivity derived for the barotropic, “single-layer” example in section 2. Inserting the formula for local diffusivity κ in (13) into the squeeze dispersion formula $\kappa_e = \langle h \rangle \langle \kappa/h \rangle$ yields

$$\kappa_e(\sigma_i) = \left\langle \frac{1}{N_i^2} \right\rangle \langle \Gamma \epsilon_i \rangle. \quad (16)$$

$$= -\frac{\rho_0}{g\Delta\sigma} \langle \Delta\zeta_i \rangle \langle \Gamma \epsilon_i \rangle. \quad (17)$$

The ratio between the passage-averaged effective diffusivity (17) and the average local diffusivity,

$$\frac{\kappa_e}{\langle \kappa \rangle} = \frac{\langle \Delta\zeta_i \rangle \langle \epsilon_i \rangle}{\langle \Delta\zeta_i \epsilon_i \rangle}, \quad (18)$$

makes clear how substantial positive or negative correlations between turbulent mixing represented by ϵ_i and squeezing represented by $\Delta\zeta_i$ imply a substantial difference between turbulent buoyancy flux and the associated effective diffusivity, and the average local diffusivity. In other words, $\kappa_e/\langle \kappa \rangle \geq 1$ implies a correlation between large ϵ_i (mixing) and small $\Delta\zeta_i$ (squeezing).

The layerwise effective diffusivity in (17) and ratio $\kappa_e/\langle \kappa \rangle$ in (18) are plotted in Figures 3e and 3f. $\kappa_e/\langle \kappa \rangle$ varies from 0.5–3 and is greater than unity more often than not. The substantial discrepancy between the isopycnal-averaged local diffusivity and the effective squeeze diffusivity across some isopycnals implies that strain substantially affects total tracer dispersion in the Samoan passage.

5. Conclusions

The importance of squeeze dispersion on oceanic diapycnal mixing depends on (i) the magnitude of oceanic vertical strain and squeezing and (ii) correlations between squeezing and diapycnal turbulence. Squeezing is often weak in mesoscale oceanic flows, being proportional to Rossby number in quasi-geostrophic flows or the nonlinearity of internal wave fields. Yet plausible dynamical mechanisms may link mixing and strain: for example, squeezing and intense turbulent mixing are co-located over mountainous bathymetry in the Samoan Passage. Numerical simulations suggest that large-scale strain may enhance turbulent intensity and mixing in preexisting shear layers (Kaminski, 2016). On the other hand, Alford and Pinkel (2000) find a *negative* correlation between squeezing and turbulent overturns and mixing in the near-surface ocean. Further observations and simulations are needed to determine the relationship between oceanic strain and turbulent mixing throughout the water column, especially where turbulence is strong and κ is large.

The effective diffusivity in (10) that arises in the thickness-weighted-average tracer evolution equation derived in section 3 does not necessarily describe the evolution of other average tracer distributions. Take the Eulerian average, for example: the Eulerian average tracer flux due to squeeze dispersion may include

contributions both from the modified Eulerian average diffusive tracer flux and the Eulerian average advective flux. Both of these are proportional to κ in nonturbulent squeeze dispersion processes. In general, both the average tracer distribution and its effective diffusivity depend on whether the average is Eulerian or a thickness-weighted average in buoyancy coordinates.

The squeeze dispersion effective diffusivity in (1) and (10) implies that the bulk diffusivity of oceanic tracers is estimated by averaging turbulent buoyancy flux and dividing by thickness-weighted-average buoyancy gradient. In section 4, we approximate the turbulent buoyancy flux with $\Gamma\epsilon$, where Γ is the mixing coefficient and ϵ is the turbulent kinetic energy dissipation rate. We then use the instantaneous buoyancy gradient N^2 to estimate the thickness-weighted-average buoyancy gradient $1/\langle 1/N^2 \rangle$, so that the ratio between turbulent buoyancy flux and thickness-weighted-average buoyancy gradient expressed by (1) and (10) becomes

$$\kappa_e = \left\langle \frac{1}{N^2} \right\rangle \langle \Gamma\epsilon \rangle, \quad (19)$$

where the angle brackets again denote an average in density space, or on an isopycnal. The dependence of the effective squeeze dispersion diffusivity (19) on the average turbulent buoyancy flux $\langle \Gamma\epsilon \rangle$ is consistent, for example, with the logic used by Voet et al. (2015) to compare the average in situ turbulent heat flux with a bulk estimate of heat flux from the temperature distribution in the Samoan passage. In section 4, we develop a technique to coarse-grain the Samoan passage observations reported in Alford et al. (2013) and Voet et al. (2015) to evaluate equation (19) and interpret its implications for tracer dispersion.

Squeeze dispersion is not shear dispersion: squeeze dispersion is proportional to diffusivity while shear dispersion is inversely proportional to diffusivity. Squeeze dispersion requires velocity gradients parallel to the direction of dispersion, while shear dispersion requires only a velocity gradient perpendicular to the direction of the tracer dispersion. Vertical oceanic shear dispersion, for example, is associated with lateral variations in vertical velocity and has an effect that is inversely proportional to lateral diffusivity. But vertical squeeze dispersion persists under vanishing lateral diffusivity and is proportional to the strength of the vertical diffusivity.

The effective diffusivity for large-scale tracers in equations (1) and (10) implies that models that use the local diffusivity but do not fully resolve oceanic strain may underpredict oceanic tracer dispersion. In other words, the parameterization of diapycnal mixing in coarse resolution models should take unresolved squeezing into account.

Finally, squeeze dispersion may also be important in other, nonoceanic laminar flows such as confined low Reynolds number flows. In these cases, the thickness h that appears in equation (1) and (10) should be interpreted as the separation between material surfaces.

Acknowledgments

Discussions with William R. Young, Jennifer MacKinnon, Carl Wunsch, Jim Ledwell, and Trevor McDougall were helpful in writing this manuscript. G. L. W. was supported by the NOAA Climate and Global Change Postdoctoral Fellowship Program, administered by UCAR's Cooperative Programs for the Advancement of Earth System Sciences. Samoan Passage research was funded by the National Science Foundation under grants OCE-1029268, OCE-1029483, and OCE-1657795. Julia code and notebooks to generate Figures 2 and 3 can be found at the website <https://github.com/glwagner/SqueezeDispersionGRL>.

References

- Alford, M. H., Girton, J. B., Voet, G., Carter, G. S., Mickett, J. B., & Klymak, J. M. (2013). Turbulent mixing and hydraulic control of abyssal water in the Samoan Passage. *Geophysical Research Letters*, 40, 4668–4674. <https://doi.org/10.1002/grl.50684>
- Alford, M. H., & Pinkel, R. (2000). Observations of overturning in the thermocline: The context of ocean mixing. *Journal of Physical Oceanography*, 30(5), 805–832. [https://doi.org/10.1175/1520-0485\(2000\)030<0805:OOITT>2.0.CO;2](https://doi.org/10.1175/1520-0485(2000)030<0805:OOITT>2.0.CO;2)
- Aris, R. (1956). On the dispersion of a solute in a fluid flowing through a tube. *Proceedings of the Royal Society A*, 235(1200), 67–77. <https://doi.org/10.1088/rspa.1956.0065>
- Davis, R. E. (1994). Diapycnal mixing in the ocean: Equations for large-scale budgets. *Journal of Physical Oceanography*, 24(4), 777–800. [https://doi.org/10.1175/1520-0485\(1994\)024<0777:DMTOE>2.0.CO;2](https://doi.org/10.1175/1520-0485(1994)024<0777:DMTOE>2.0.CO;2)
- De Szoeke, R. A., & Bennett, A. F. (1993). Microstructure fluxes across density surfaces. *Journal of Physical Oceanography*, 23(10), 2254–2264. [https://doi.org/10.1175/1520-0485\(1993\)023%3C2254:MFADS%3E2.0.CO;2](https://doi.org/10.1175/1520-0485(1993)023%3C2254:MFADS%3E2.0.CO;2)
- Gent, P. R., & McWilliams, J. C. (1990). Isopycnal mixing in ocean circulation models. *Journal of Physical Oceanography*, 20(1), 150–155. [https://doi.org/10.1175/1520-0485\(1990\)020<0150:IMOCM>2.0.CO;2](https://doi.org/10.1175/1520-0485(1990)020<0150:IMOCM>2.0.CO;2)
- Gregg, M. (1998). Estimation and geography of diapycnal mixing in the stratified ocean. *Physical Processes in Lakes and Oceans*, 54, 305–338. <https://doi.org/10.1029/CE054p0305>
- Kaminski, A. K. (2016). Linear optimal perturbations and transition to turbulence in strongly-stratified shear flows (Unpublished doctoral dissertation) (PhD thesis), University of Cambridge.
- Ledwell, J., Montgomery, E., Polzin, K., Laurent, L. S., Schmitt, R., & Toole, J. (2000). Evidence for enhanced mixing over rough topography in the abyssal ocean. *Nature*, 403(6766), 179.
- Ledwell, J., St. Laurent, L., Girton, J., & Toole, J. (2011). Diapycnal mixing in the Antarctic circumpolar current. *Journal of Physical Oceanography*, 41(1), 241–246. <https://doi.org/10.1175/2010JPO4557.1>
- Mashayek, A., Ferrari, R., Merrifield, S., Ledwell, J. R., St Laurent, L., & Naveira Garabato, A. (2017). Topographic enhancement of vertical turbulent mixing in the Southern Ocean. *Nature Communications*, 8, 14197. <https://doi.org/10.1038/ncomms14197>

- McDougall, T. J., & McIntosh, P. C. (2001). The temporal-residual-mean velocity. Part II: Isopycnal interpretation and the tracer and momentum equations. *Journal of Physical Oceanography*, 31(5), 1222–1246. [https://doi.org/10.1175/1520-0485\(2001\)031<1222:TTRMVP>2.0.CO;2](https://doi.org/10.1175/1520-0485(2001)031<1222:TTRMVP>2.0.CO;2)
- Moffatt, H. (1983). Transport effects associated with turbulence with particular attention to the influence of helicity. *Reports on Progress in Physics*, 46(5), 621–664.
- Oakey, N., & Elliott, J. (1982). Dissipation within the surface mixed layer. *Journal of Physical Oceanography*, 12(2), 171–185. [https://doi.org/10.1175/1520-0485\(1982\)012<0171:DWTSMML>2.0.CO;2](https://doi.org/10.1175/1520-0485(1982)012<0171:DWTSMML>2.0.CO;2)
- Osborn, T. (1980). Estimates of the local rate of vertical diffusion from dissipation measurements. *Journal of Physical Oceanography*, 10(1), 83–89. [https://doi.org/10.1175/1520-0485\(1980\)010<0083:EOTLRO>2.0.CO;2](https://doi.org/10.1175/1520-0485(1980)010<0083:EOTLRO>2.0.CO;2)
- Redi, M. H. (1982). Oceanic isopycnal mixing by coordinate rotation. *Journal of Physical Oceanography*, 12(10), 1154–1158. [https://doi.org/10.1175/1520-0485\(1982\)012<1154:OIMBCR>2.0.CO;2](https://doi.org/10.1175/1520-0485(1982)012<1154:OIMBCR>2.0.CO;2)
- St. Laurent, L., Naveira Garabato, A. C., Ledwell, J. R., Thurnherr, A. M., Toole, J. M., & Watson, A. J. (2012). Turbulence and diapycnal mixing in Drake Passage. *Journal of Physical Oceanography*, 42(12), 2143–2152. <https://doi.org/10.1175/JPO-D-12-027.1>
- Voet, G., Girton, J. B., Alford, M. H., Carter, G. S., Klymak, J. M., & Mickett, J. B. (2015). Pathways, volume transport, and mixing of abyssal water in the Samoan Passage. *Journal of Physical Oceanography*, 45(2), 562–588. <https://doi.org/10.1175/JPO-D-14-0096.1>
- Watson, A. J., Ledwell, J. R., Messias, M.-J., King, B. A., Mackay, N., Meredith, M. P., et al. (2013). Rapid cross-density ocean mixing at mid-depths in the Drake Passage measured by tracer release. *Nature*, 501(7467), 408. <https://doi.org/10.1038/nature12432>
- Young, W. R. (2012). An exact thickness-weighted average formulation of the Boussinesq equations. *Journal of Physical Oceanography*, 42(5), 692–707. <https://doi.org/10.1175/JPO-D-11-0102.1>